energies

MDPI

Article

Experimental Attempts to Investigate the Influence of Petrographic Properties on Drying Characteristics of Lignite in Superheated Steam Atmosphere

Anna Sciazko [1], Yosuke Komatsu [2,3,*], Marcin Zakrzewski [1], Taro Akiyama [3], Akira Hashimoto [3], Naoki Shikazono [3], Shozo Kaneko [3], Shinji Kimijima [3,4], Janusz S. Szmyd [1] and Yoshinori Kobayashi [3]

1 AGH University of Science and Technology, Department of Fundamental Research in Energy Engineering, Krakow 30-059, Poland; sciazko@agh.edu.pl (A.S.); zakrzews@agh.edu.pl (M.Z.); janusz.szmyd@agh.edu.pl (J.S.S.)
2 Shibaura Institute of Technology, Division of Regional Environment Systems, Saitama 337-8570, Japan
3 The University of Tokyo, Institute of Industrial Science, Tokyo 153-8505, Japan; t-aki@iis.u-tokyo.ac.jp (T.A.); a-hashi@iis.u-tokyo.ac.jp (A.H.); shika@iis.u-tokyo.ac.jp (N.S.); s-kaneko@iis.u-tokyo.ac.jp (S.K.); kimi@sic.shibaura-it.ac.jp (S.K.); yosikoba@iis.u-tokyo.ac.jp (Y.K.)
4 Shibaura Institute of Technology, Department of Machinery and Control Systems, Saitama 337-8570, Japan
* Correspondence: m610101@sic.shibaura-it.ac.jp; Tel.: +81-48-687-5174

Academic Editor: Jean-Pierre Bédécarrats
Received: 28 February 2016; Accepted: 4 May 2016; Published: 16 May 2016

Abstract: A superheated steam fluidized bed dryer (SSFBD) in a self-heat recuperative configuration has a great potential of improving thermal efficiency of a lignite-fired power plant by recovering both of latent heat of vaporization of water kept in the fuel and part of sensible heat during the fuel processing. However, the optimal design of the dryer requires the fundamental knowledge of drying characteristics in respect to the individual properties of the utilized fuel. Experimental investigation to determine the correlation between a specific coal properties originated from geological background and its drying characteristics is thus the major concern in this paper. The investigated lignite is a representative of Turoszow deposit in Poland. Experimental attempts unveiling drying kinetics were carried out for 5 mm and 10 mm diameter spherical samples in the superheated steam atmosphere in the temperature range of 110 °C–170 °C. Simultaneous and continuous measurements of changes in weight, surface and interior temperatures and appearance on each tested sample were carried out for describing drying behavior. Analytical investigation was applied to explain the drying characteristics, which are strongly affected by the individual properties of coal and the inherent ash composition.

Keywords: Turow lignite; superheated steam drying; drying characteristic; low-rank coal (LRC); lignite upgrading

1. Introduction

Lignite (brown coal or low-rank coal (LRC)) deposits occupy one-fourth of widespread coal resources in the entire world and play significant role economically and politically in countries where its share in energy mix becomes a dominative level [1]. Unfavorable limitation of lignite for transportation or storage, due to high moisture content (typically 40%–70% of water in mass), precludes the enhancement of lignite utilization. Thus, an appropriate treatment is needed for coke production and the limited utilization in power generation sector.

Additionally, high moisture content deteriorates the thermal efficiency of power generation sector, in particular combustion process, due to the heat loss originated from the vaporization of large amount of water contained within this fuel carrier. Water removal technology for lignite has thus been attended

as a solution for efficient utilization. Among various types of proposed drying systems by means of mechanical, thermal or chemical methods [2], superheated steam fluidized bed drying (SSFBD) enables recovering latent heat from the water vaporization with minimized heat loss and is potentially capable of recovering sensible heat in a self-heat recuperative configuration [3,4]. The superheated steam based drying systems were proposed and investigated for various materials [5–9].

Superheated steam as drying medium eliminates hazards in lignite drying: oxidation of lignite and its consequences of spontaneous ignition, environmental pollution emissions, *etc.* The other feature is improving the gridability index of upgraded lignite. The most attractive perspective of this drying medium is in principle saving more energy consumption compared with other drying medium such as hot gas: this is the result of high heat transfer coefficient, especially above the inversion temperature. Fluidized bed drying, traditionally used in various field of industries, has advantageous features in enhancing heat and mass transfer phenomena. It is also said that the SSFBD can be a suitable dryer in handling process of drying in terms of large scale operation [4,10,11]. The size and shape of objects occur in the process can suppress the quality of fluidization [4,10,11].

Installation of such a drying system into a conventional lignite-fired power station is attractive in revolutionary enhancing their thermal efficiency. Thus, attempts have been made for its commercialization for a long time, but the potential of the system is not fully developed yet. Noteworthy perspective in this issue is that most of those lignite-fired power plants are operated with lignite excavated from the regions where they are located. Investigations on drying kinetics of a particular grade of coal from the place in which a power station is allocated, are certainly important. Bongers *et al.* [12,13] have studied the drying kinetics of Loy Yang lignite at pressurized conditions together with those of Morwell lignite. Looi *et al.* [14] have studied the drying characteristics of Victorian lignite in pressurized superheated steam. Shi *et al.* [15] have investigated the drying behavior of Pongzhuang lignite excavated in China. The research group of the authors of the present paper carried unique experimentation for studying the drying characteristics of Loy Yang (Australia) and Belchatow (Poland) lignite [16–18]. Thanks to those distinct works, it is clearly observed that the individual drying behavior vary significantly among different types of lignite. This observation fits to the statement by Pikon and Mujumdar [19]: "Superheated steam seems to provide all the required advantages but few vendors have developed these technologies for coal and for large-scale operations necessary. The drying conditions will need to be optimized for specific grades of coal and also the utilization of the product."

Therefore, locally and geologically deviated coal properties have to be concerned as the influential factor for drying characteristics. The individuality of lignite may cause the significant difficulty of water removal in the SSFBD system. For instance, the porosity given by the structure of coal originated from the coalification of organic matters and formed in sedimentation is not discussed yet, though they can suppress the attracting characteristics of evaporative drying that enhance the heat and mass transfer. In this content, the diversity of coal properties from a certain mine in respect to drying characteristics must be unveiled for optimizing a dryer to this particular energy carrier. From this perspective lignite drying tests were examined in the superheated steam atmosphere using lignite samples that have inhomogeneous properties along the seam depth. The present study attempts to clarify the correlation between geological and petrographic properties and drying characteristics of lignite originated from the Turoszow deposit in Poland.

2. Features of Lignite

2.1. Geological Origin

Figure 1 shows the allocation of samples used in the present experimentation. The investigated lignite is representative for Turoszow deposits situated in the extreme southwestern part of Poland.

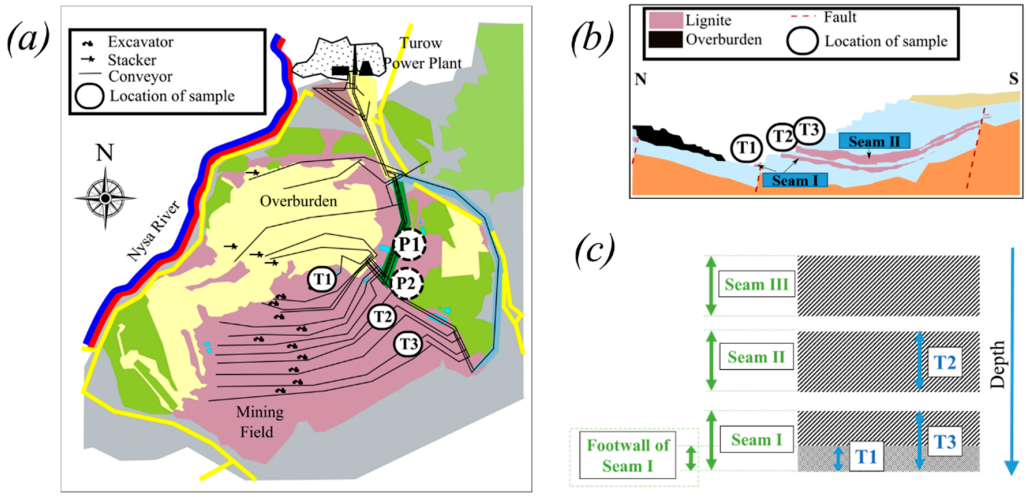

Figure 1. (**a**) Overview of Turow mine; (**b**) profile of the mine; and (**c**) scheme of sample location [20].

The samples represents two different seams which currently are under exploitation and have industrial value: Seam I in the stratigraphic third group of Ścinawa lignite seams (ŚLS-3) (14 m profile core sample and footwall sample designated as Samples T3 and T1, respectively) and Seam II belonging to the second group of Lusatian lignite seams (LLS-2) (18 m profile core sample designated as Sample T2) [21]. ŚLS-3 and LLS-2 are the structures that has originated from Lower Miocene and between lower and middle Miocene, respectively [21]. Dominating compositions of each seam were presented in Table 1 together with the specifications of examined samples. The exemplary lignite seam profiles of Seams I and II are illustrated in Figure 2 [22].

Table 1. Details of lignite samples.

Sample	Depth (m.a.s.l.)	Thickness of Sample (m)	Thickness of Seam (m)	Seam	Dominating Type of Lignite
T1	35	4	12	I	Footwall sample: detritic coal, high contamination
T2	123	18	18	II	Xylitic and detritic coal
T3	126	14	14	I	Detritic coal

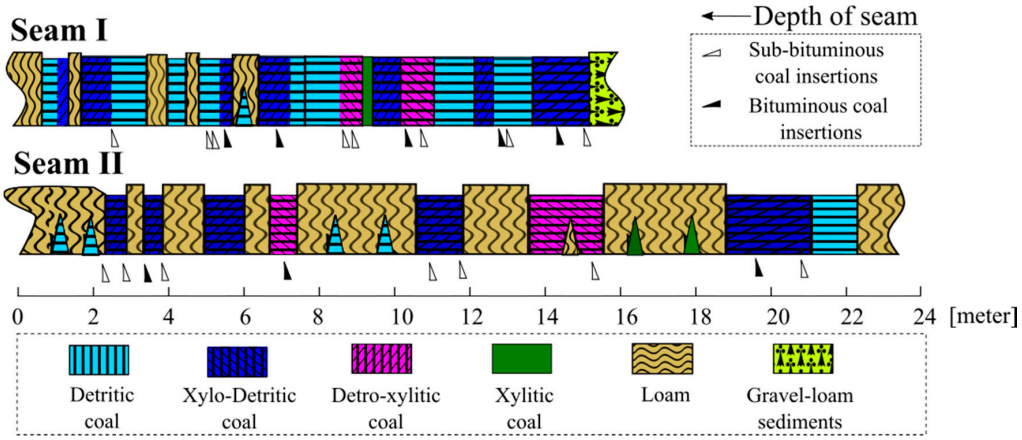

Figure 2. An exemplary of seam's petrographic profile found in Seams I and II [22].

The profiles were taken in the neighborhood of drilling points of Samples T2 and T3. The locations of the samples taken were correspondingly presented in Figure 1a: the point P1 for Seam I profile and

the point P2 for Seam II profile. The variety of petrographic lithotype textures can be observed in both of their profiles: detritic, xylitic, detro-xylitic and xylo-detritic coals. Detritic coal is humic groundmass characterized by the fine-graded, usually homogenous structure of organic matter. Xylitic lignite has a matrix of detrital coal with fragments composed of carbonized wood—xylite. The xylites consist at least 90% of this lithotype; therefore, layered structure of wood is clearly visible. Xylo-detritic and detro-xylitic lignites are combination of two previous lithotypes. It has to be noted that opposed to the nomenclature, the xylo-detritic coal is composed from higher share of detrial matrix than xylites. Analogically detro-xylitic lignite contains more xylitic particles than fine-detrial matrix [23]. Among of texture of Turow seams, detritic and xylo-detritic coal are dominant in Seams I and II and similar petrographic composition and geological structures can be observed in both of them. Significant number of sub- and bituminous coal insertion can be found in the seams' profiles. Seam I has more uniform structure compared to Seam II. On the other hand, high contamination of the loam can be noticed in the footwall of Seam I.

2.2. Properties of Lignite

The properties of the lignite sample used in the present experimentation are provided in Figure 3. Proximate and ultimate analyses have been carried out in accordance with the Japanese Industrial Standards (JIS M).

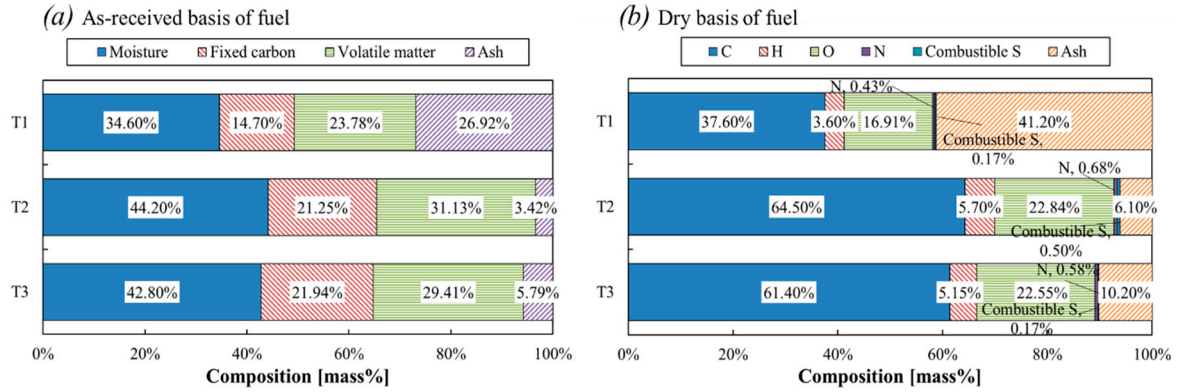

Figure 3. (**a**) Proximate; and (**b**) ultimate analyses of lignite samples used in the present experimentation.

Samples T1 and T3 are located in the same seam, Seam I. However, the allocation of Sample T1 was the footwall as mentioned while Sample T3 represents the whole core profile of Seam I. Ash content in Sample T1, counting the contaminations and non-organic mineral matter, is likely the highest among all the tested samples. The amount of natural moisture of Sample T1 is then the lowest among them, while that of T2 and T3 are very similar to each other (the amount of water in Sample T2 is slightly larger than one in T3). Contents of elemental matters in Samples T2 and T3 are alike (slightly higher composition of ash in Sample T3), though the seams that Samples T2 and T3 belong to are originated from different roots. In Table 2, the density of lignite (as-received basis and dry basis) and consisted ash measured in JIS method were compared for Samples T1, T2 and T3. The density of Sample T1 is higher than those of any others. This may come from the large amount of contamination classified as ash in Sample T1, though the density of ash from Sample T2 is the heaviest.

Table 2. Density of lignite samples and their ash.

Property	T1	T2	T3
Dry Bulk density of coal (kg· m^{-3})	766	613	636
Density of dry matter in coal (kg· m^{-3})	1827	1486	1436
Ash's density (kg· m^{-3})	2315	3120	2866

3. Experimental

3.1. Sample Preparation

The experiment was conducted with spherical lignite samples of 5 mm and 10 mm in diameter. Firstly, the spherically shaped object with approximately doubled diameter was cut from the randomly chosen piece of lignite. The shape of the sample was polished on a plate by rolling in a hole precisely punched with an electrical discharged machining process. Polishing was carried out step by step in several sizes of holes and was regulated to the desired size. Finally, the size of the sample was adjusted to the particular diameters: 5 ± 0.05 mm and 10 ± 0.05 mm. Thermocouples were attached to the precisely smoothed sample for the purpose of measuring temperatures s inside the sphere: a pair of thermocouple for the 5 mm sample and two pairs of thermocouple for the 10 mm sample. The hole, in which thermocouple was attached, was made with a 0.2 mm drill. For the 5 mm sample, the depth of the hole is 2.5 mm, at which the tip of the thermocouple reaches the center of the sample. For the 10 mm sample, the depth of the holes was 2.5 mm and 5 mm, which corresponds to the middle point (midpoint, half of the radius) and center of the sample, respectively. The used thermocouples were K-type thermocouples composed of two 0.08 mm wires made of chromel and alumel insulated with Silica-based material. Thermocouples were additionally used to hang sample on the thin glass rod of which the diameter is 0.5 mm.

3.2. Experimental Setup

After the preparation, the sample was set in the test section, where lignite was dried in a superheated steam atmosphere. Figure 4a shows the configuration of the experimental apparatus. The cylindrical test section, of which the diameter is 133 mm and the height is 152 mm, was operated with heaters providing the uniform temperature in the testing zone. The heaters were located on the bottom of the test section, around the outer wall and on the cover of the test section. Pure water was degassed, pumped up by a liquid delivery pump and provided to an evaporator and then a superheater. The superheated steam was sent into the top of the test section, to which a baffle plate was attached to disperse the supplied steam into the entire test section, and exhausted from the bottom by a fan. The sample weight, its surface and interior temperatures (both center and midpoint) were measured for the observation and discussion of the drying characteristics. The weight was measured with an electronic balance having a resolution of 0.1 mg. The electronic balance was connected with a metal suspension wire, on which the glass rod with the sample was hanged. The suspension wire was surrounded by a protective acryl pipe. Air was supplied into the acryl pipe attached under the electronic balance at the rate of 0.6 $dm^3 \cdot min^{-1}$, in order to stabilize the temperature and flow inside the pipe and ensure accurate weight measurement.

The measurements of the sample temperature profile included measurements of the temperatures on the surface, center and midpoint of the lignite particle. The temperatures inside the sample (center and midpoint) were checked by the K-type thermocouples attached as explained above. The surface temperature was measured by a thermography camera equipped with infrared bolometers in the range of wavelength detection from 8 μm to 12 μm. A detailed configuration of the outline and cross-section of the thermography devices and test section is presented in Figure 4c. The thermography camera was connected to the test section by an optical path starting from the window in the test section cylinder. The heat loss to the ambient was reduced by heating of the optical path. The installed heater also reduced the possibility of steam condensation on the film separating the test section from the ambient and the path itself. The 10 μm thick polymethylpentene film was set in the optical path at an inclination of 10° to avoid infrared reflection. The installed film had the heatproof temperature 180 °C and its average transmittance in the range of wavelengths from 8 μm to 12 μm was equal to 90%. Additionally, all of the inner surfaces of test section and optical path were sprayed with the black body paint with emissivity of 0.94 in order to ensure the correct thermography measurement. Thermography was calibrated on the basis of the assumptions of constant sample emissivity and

constant test section temperature as well as the sample characteristic temperatures. Sample temperature profile were the characteristic points of drying process: evaporation of the free water in 100 °C and reaching test temperature in the final stage.

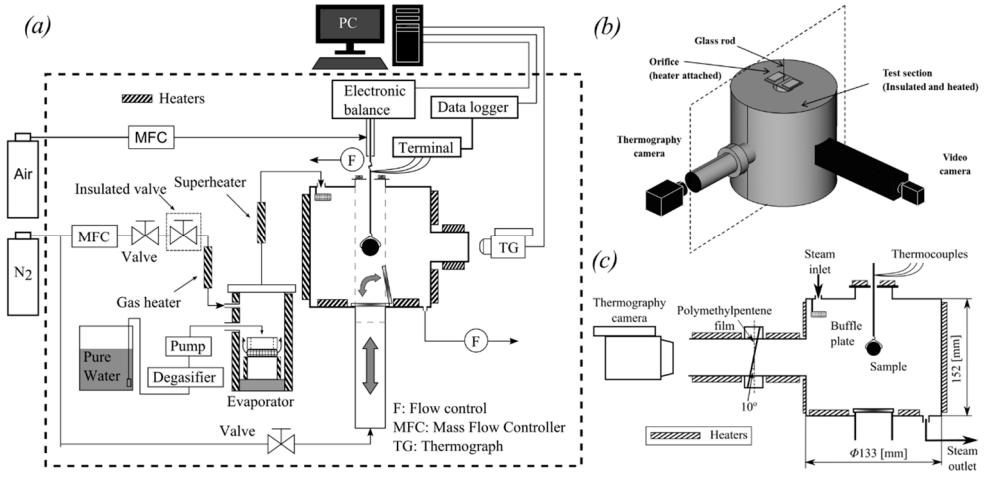

Figure 4. (**a**) The configuration of the experimental setup; (**b**) measurement of the surface temperature by thermography camera and the observation of the sample surface by a video camera; and (**c**) the geometrical specification of the measurement of the surface temperature of a coal sample [18].

Figure 4b also presents the position of the video camera that was used to observe the changes in the surface of the lignite particle. The camera optical path is connected to the test section chamber. The optical paths of video camera and thermography camera are perpendicular to each other, what makes possible the simultaneous recording of different sample properties. The additional heater was provided for the glass window between the test section and camera optical path.

To eliminate the influence of the ambient condition and prevent air flow circulation, the experimental equipment was enclosed with polyvinyl chloride sheets, which are pointed by a dotted line in Figure 4a. The relative humidity in the enclosure was maintained at over 45% to eliminate the effects of static electricity, which disturbs the measurement of the weight. Moreover, in order to minimize the static electricity influence antistatic spray was frequently used and zero-ground cables were installed.

3.3. Experimental Procedure

The samples were dried in the test section where the temperature of the chamber was kept at 110, 130, 150 and 170 °C in the atmospheric superheated steam condition. As the drying temperature is maintained under 180 °C, it is assumed that volatilization and the decomposition of functional groups are not occurring [24,25]. Thus, it can be assumed that the change in the weight is caused by moisture removal. The experimental procedure was started by heating up the test section under the nitrogen flow. When the test temperature was reached, the nitrogen flow was replaced by the flow of superheated steam. Steam was fed at an average velocity of 0.02 $m \cdot s^{-1}$ in the test section, which corresponds to 8 $cm^3 \cdot min^{-1}$ of water flowing to the evaporator. The Reynolds numbers in this condition were about 3.2 and 6.4 for 5 mm and 10 mm samples, respectively. The adopted laminar flow conditions enable the precise measurement of the weight.

The sample was placed in the test section after the stabilization of the experimental condition. To define the exact moment of the start of superheated steam drying, a sample set on the glass rod was isolated from the superheated steam atmosphere by raising the starting pipe. During this procedure, the starting pipe was filled with nitrogen. After lowering the starting pipe and exposing the sample to the superheated steam, changes in weight W and temperature T profile of the lignite particle were consequently and simultaneously recorded in 1 s intervals. The completion of the superheated drying

process was then judged to have been obtained when a change in weight became less than 0.1 mg/min, which was less than 0.01% of the dried sample weight. In order to verify the amount of residual water, the drying medium was switched to nitrogen, and the sample was dried for a certain time (depending on the test temperature and the size of the sample) enough to evaporate any additional moisture. The weight of the sample after nitrogen drying was regarded as the weight of the coal contained in the lignite (dry basis), W_c. The weight of the water in the lignite, W_w was determined by subtracting W_c from the initial weight of the sample, W_{ini}. For each size of the sample (5 mm and 10 mm), the experiments were conducted at least 3 times at each test temperature. Here, another important definition of the specific use of terms that should be noted; in this study, dry basis moisture content X is defined as the ratio of the water weight W_w (kg) to the weight of the dried coal W_c (kg):

$$X = \frac{W_w}{W_c} \tag{1}$$

On the other hand, the ratio of the weight of the water to the initial weight of the sample is defined as the water percentage (WP) mass%:

$$WP = \frac{W_w}{W_{ini}} \times 100 = \frac{W_w}{W_{w,ini} + W_c} \times 100 \tag{2}$$

where W_{ini} is the initial weight of the sample (kg) and $W_{w,ini}$ is the initial weight of the water (kg).

4. Results and Discussion

4.1. Lignite Drying Behavior in Superheated Steam

Figure 5 shows the exemplary drying behavior of Sample T1 in the superheated steam. The indicated case was the examination of drying with 10 mm samples in the test temperature 150 °C. The test was repeated for several spherical samples, which were made of randomly chosen blocks of lignite T1 and three exemplary tests are shown here. To describe drying behavior, the change in the sample's weight (Figure 5a), temperature profile (Figure 5b), moisture content (Figure 5c) and the drying rate (Figure 5d) are presented. The drying rate curve plots are drawn in Figure 6. Figure 7 shows the surface observation (both initial and final states) of a sample at each test. Table 3 lists other importance: the initial water percentage (WP_{ini}), the residual WP, the steam drying time and the initial drying rate found at each test. In general, drying behavior of lignite, which is a material with hydrophilic porous structure, can be categorized into three periods: pre-heating period (T < 100 °C) when stem is condensate on the sample surface, constant drying rate period (CDRP) (T = 100 °C) and decreasing drying rate period (DDRP) (T > 100 °C). Note that the drying behavior of Turow lignite follows this manner. However, the CDRP is generally very short, though this depends on initial moisture content of the sample. As can be seen in the obtained results, the variations of the initial water are wide as resulted in 26.8%–47.9%. Therefore, the drying behavior differs to each other among the three represented tests. With lower moisture content sample (Test 1), which has a heavier weight, the pre-heating period and CDRP finishes faster than others, and then the increase of the sample's temperature (both the surface and the center) starts earlier than others and the raise is more rapid.

Table 3. Initial and residual water percentages (WP) and steam drying time of 10 mm sample at the test temperature of 150 °C.

Property	Test 1	Test 2	Test 3
Initial water (mass%)	26.8	38.9	47.9
Residual water (mass%)	0.7	1.5	1.4
Steam drying time (min)	42.1	57.6	58.2
Initial drying rate ($\times 10^{-4} \cdot s^{-1}$)	3.37	4.69	6.07

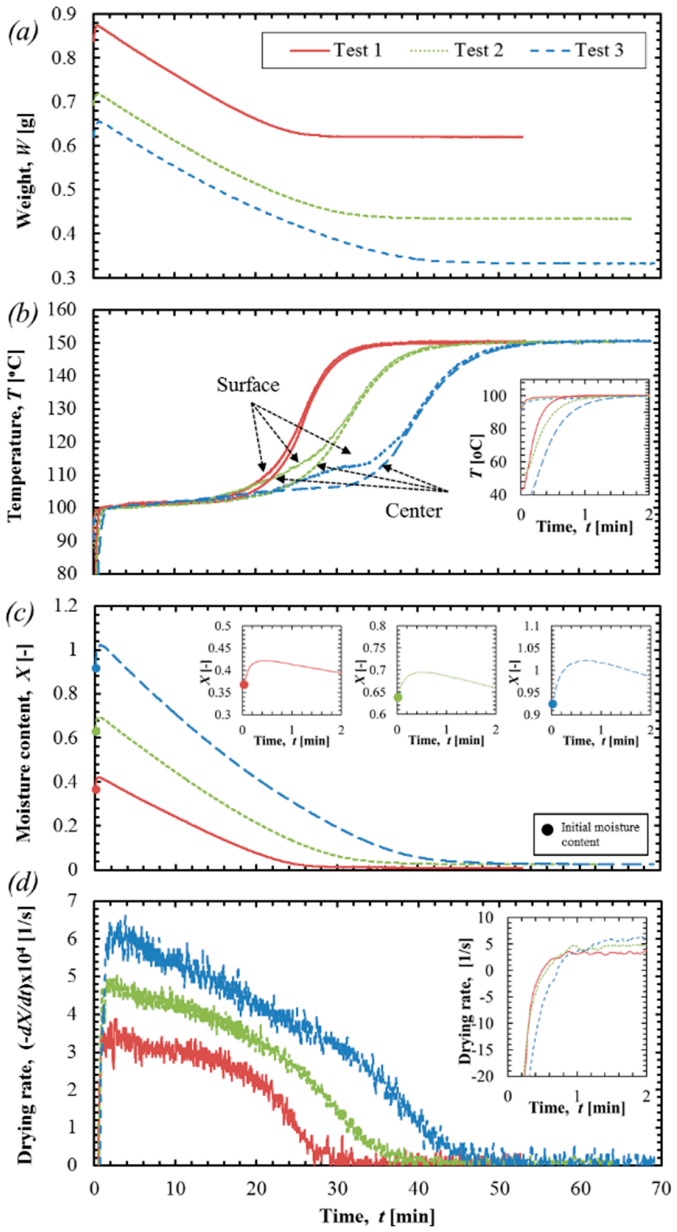

Figure 5. Exemplary drying characteristics of Sample T1 in superheated steam: 10 mm sample used in test temperature at 150 °C, change in: (**a**) weight; (**b**) temperature profiles; (**c**) moisture content; and (**d**) drying rate.

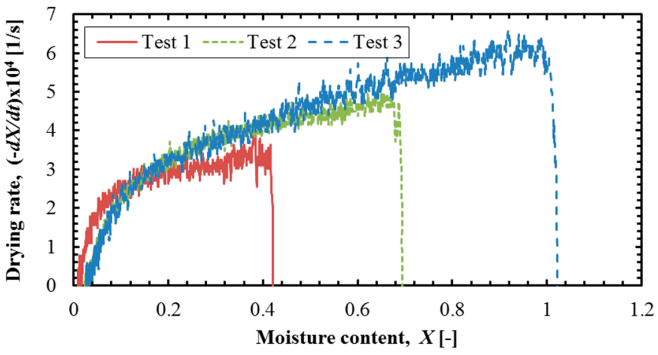

Figure 6. Drying rate curve plot of 10 mm sample at the test temperature of 150 °C.

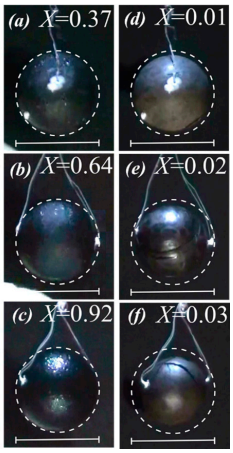

Figure 7. Sample surface: (**a**) initial; (**b**) final states in Test 1; (**c**) initial; (**d**) final states in Test 2; (**e**) initial; and (**f**) final states in Test 3.

Thus, the drying process is completed sooner than other tests (Table 3). With Tests 2 and 3, the increase of the center temperature is gradual to that of the surface temperature in the transition from the saturation temperature to the test temperature. In Test 1, the rise of temperature at the sample center is rapid due to lower moisture content, and small temperature gradient is observed over any other instance on the transition from the saturation temperature to the test temperature. The sample with low moisture content has a heavier weight, so that the change in the weight caused by the water evaporation is quantitatively small to the weight of the dried sample. Thus, moisture content becomes smaller in the sample and it leads to the lower drying rate. This also influences the appearance of the sample, as it was shown in Figure 7. The initial and final states of all the samples in the superheated steam drying process are indicated. The white dot circle in the pictures is the outline of the initial shape of the samples. The values of moisture content at initial and final states are also indicated. When comparing the physical appearance at the final state to that of the initial state, the size of the sample becomes smaller. This can be seen in all the represented cases. Pores, in which water is kept in the sample, become vacant after the water removal and they are crushed due to thermal stress mostly in the DDRP at which the sample's surface and core temperatures start increasing from the saturation temperature to the test temperature. This behavior was previously shown [18]. The water transported from the inside sample to the shell at the CDRP might occur not as vapor, but in the form of liquid. This allows for keeping homogenous temperature distribution inside the sample. Crushing of pores is not dominant phenomena in the CDRP. As a consequence of the water removal, the sample shrinks in all the cases. The volume shrinkage at the final state was estimated; 7.7% in Test 1, 18.3% in Test 2 and 40.7% in Test 3. The degree of shrinkage on Test 3, which has highest initial water of 47.9%, is visibly more remarkable than that of Test 1, which has lowest initial water of 26.8%. High moisture content sample possesses large numbers of pores to keep that amount of water inside. Thus, the dried sample becomes significantly smaller, comparing to the initial size. In the case of the lower moisture content sample (Test 1), the shrinkage of the sample is not alike the rest of tests (Tests 2 and 3), this may be connected with ash content in the sample. The surface color of the Test 1 sample is very bright and rather grey color compared to the others (Figure 8a,d). Considering the proximate analysis, the color is resulted from the large ash content, in which silica and alumina oxides dominate over 85% of the composition. The specific gravity of ash is larger than lignite (Table 2) and this results in the heavier weight of the sample. Looking at the Figure 8b,c, cracking on the sample surface is observed in both Tests 2 and 3. This cracking occurred primarily along the one certain direction of the sample in Test 2 (Figure 8e). In the meantime, the appearance of cracks in Test 3 is more frequent than in Test 2 and is on many directions (Figure 8f). A heavier weight sample in Test 1 does have less amount of water within itself, so significant cracking on its surface was not observed.

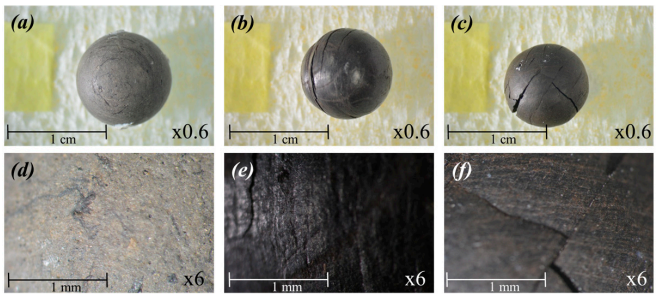

Figure 8. The samples used in: (**a**) Test 1; (**b**) Test 2; and (**c**) Test 3. Magnified pictures of the surfaces in: (**d**) Test 1; (**e**) Test 2; and (**f**) in Test 3.

Ticleanu *et al.* [26] discussed the correlation between the lithotypes of Oltenia coals and their main quality characteristic. Specifically, they presented correlations for xylitic coal, weak xylitic coal (transition between xylitic and detritic), detritic coal and clayey coal. According to [26], ash content can be used as a lithotype indicator. Generally, it was concluded that xylite and xylitic coal contains the smallest amount of ash, then higher amount of ash are correlated respectively with weak xylitic coal, detritic coal and clayed coal. This correlation is coherent with the presented observations on the samples weight, drying time, and observed structure and characterization of lithotype of each sample.

Figure 9 shows the summary of exemplary drying characteristics of Samples T1, T2 and T3 in the temperature of 170 °C of superheated steam for both 5 nm and 10 mm sample. Drying behavior of Samples T2 and T3 is very similar to what has been observed in that of Sample T1. The variation of drying behavior is wide and they differ each other. The drying rate curve plot, at each test temperature of 110, 130, 150 and 170 °C, is also summarized in Figure 10. The clearly visible influence of the particle size and superheated steam temperature was explained in previous work [18], but the additional variety from individual properties of coal is observed. Because of the diversification of the petrographic lithotype texture, it is very difficult to determine the representative characteristics of drying behavior for each case. Therefore, to understand the influence of individual lithotype, it is necessary to study the behavior of individual samples (Figures 5–7) rather than general overview of lignite T1, T2 and T3.

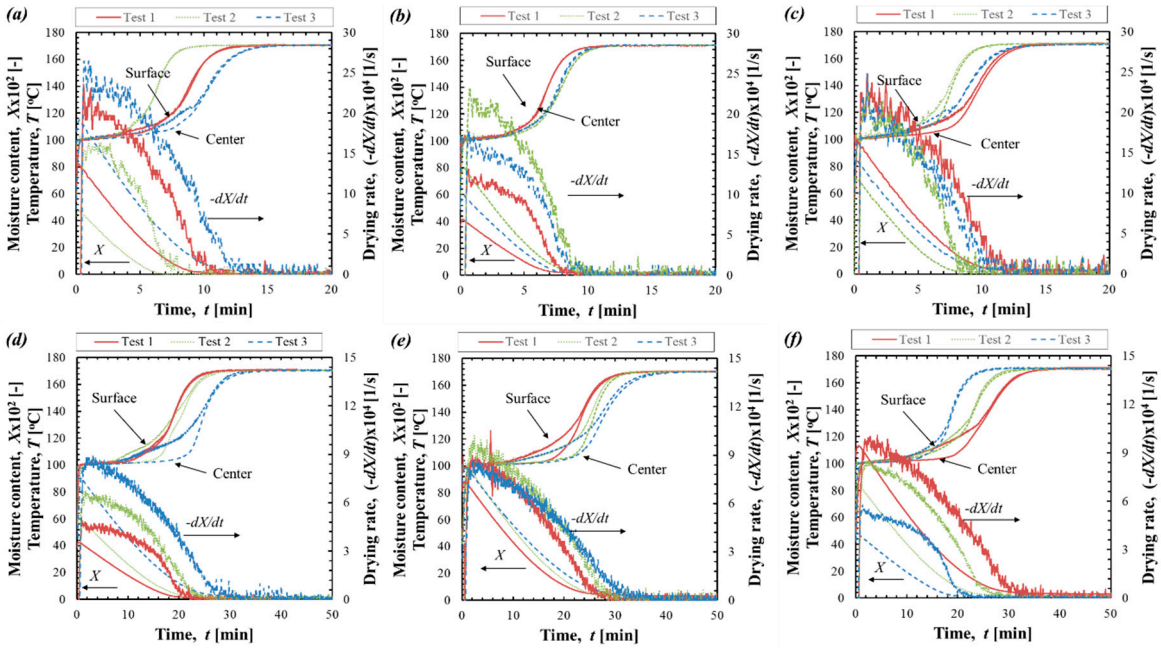

Figure 9. Exemplary drying behavior of lignite spherical sample at the test temperature of 170 °C: (**a**) T1 5 mm; (**b**) T2 5 mm; (**c**) T3 5 mm; (**d**) T1 10 mm; (**e**) T2 10 mm; and (**f**) T3 10 mm samples.

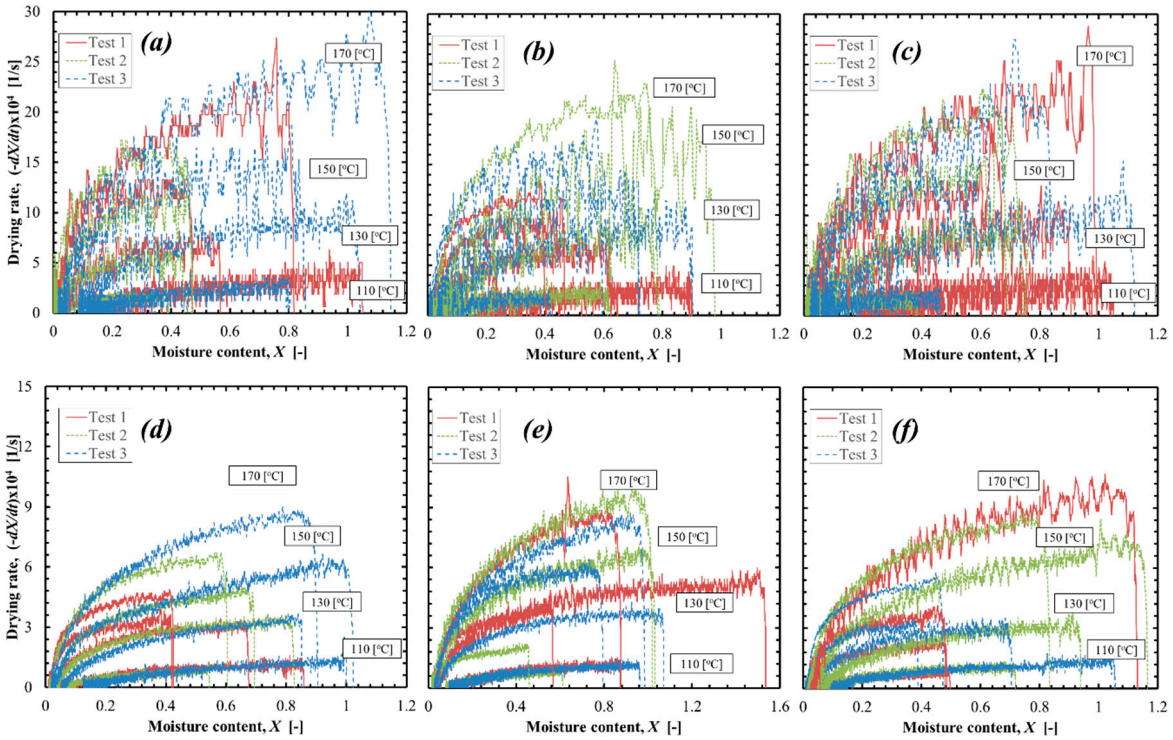

Figure 10. Drying rate curve plot for: (**a**) T1 5 mm; (**b**) T2 5 mm; (**c**) T3 5 mm; (**d**) T1 10 mm; (**e**) T2 10 mm; and (**f**) T3 10 mm samples.

4.2. Thermodynamic Evaluation of the Drying Rate at Constant Drying Rate Period

As it is well known that the heat input to the sample is consumed for the evaporation of water in the CDRP since the change in the temperature profile does not occur, the initial drying rate of the test can be thermodynamically derived. As the thermodynamic evaluation has been previously carried out and verified for lignite from the Belchatow deposit, the initial drying rate (the drying rate at the CDRP) (s^{-1}) can be derived from the following equation [18]:

$$\left(\frac{dX}{dt}\right)_{CDRP} = \frac{6h(T_{test} - T_s)}{-\Delta H \rho \varphi_{l,ini}} \frac{1}{d} \quad (3)$$

where h stands for the heat transfer coefficient ($kW \cdot m^{-2} \cdot K^{-1}$), ΔH enthalpy change of water evaporation (latent heat of the free water at 100 °C, 101.325 kPa, $\Delta H = L = 2.256\ MJ \cdot kg^{-1}$), T_{test} is the temperature of the drying medium (K), T_s is the sample surface temperature (K), ρ is the density of raw sample at initial state ($kg \cdot m^{-3}$), $\varphi_{l,ini}$ is the mass fraction of dry lignite in a sample (–) and d is the diameter of the sample (m). The detailed derivation and a method estimating the heat transfer coefficient are presented in [18]. This coefficient described by the flow velocity, the size of particle and test temperature. Figure 11 shows the consistency of the thermodynamically calculated drying rate to the experimentally obtained drying rate (at CDRP). General formula can incorporate though significant variation of properties appears; it was proven that the proposed formula is effective in prediction of the initial drying rate in the CDRP and describes well the variations observed in Figure 10. This also means that the drying rate at the CDRP is governed by the degree of superheated steam, the size of lignite as well as the initial condition of the sample, mainly WP_{ini} what was decided by the physical characteristics of the dried lignite object. The results presented in Figure 11 clearly show that Equation (3) can be applied to many types of samples lying on the broad range of WP_{ini} and the initial density.

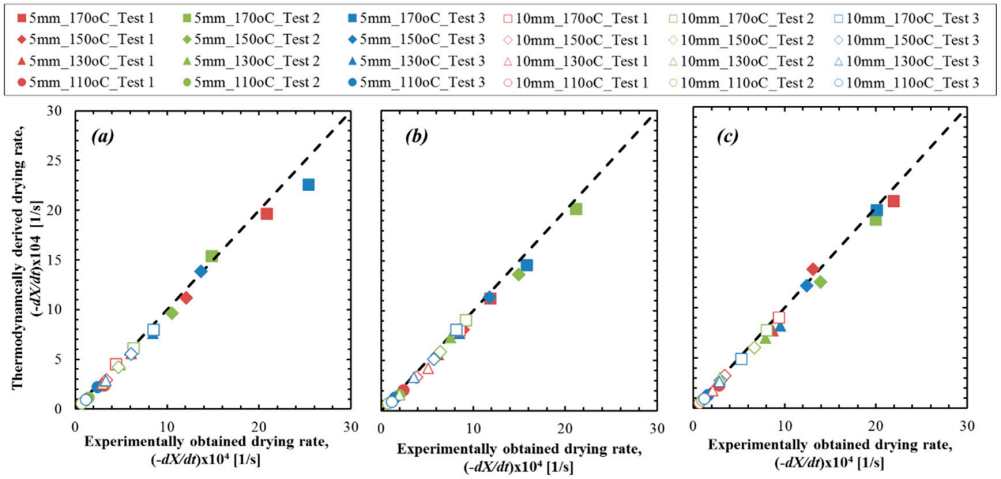

Figure 11. Comparison between the experimentally obtained drying rate and thermodynamically derived drying rate at the constant drying rate period (CDRP). The results for: (**a**) T1; (**b**) T2; and (**c**) T3 samples.

The dry bulk density ρ_b is defined as the mass of the dry lignite W_c (kg) divided by the total volume of the raw sample V_{ini} (m^3):

$$\rho_b = W_c / V_{ini} \quad (4)$$

Figure 12 shows the impact of WP_{ini} and initial density on the dry bulk density ρ_b based on the fixed volume of samples. A plane surface in Figure 12 is the theoretical space of possible values of dry bulk density from various initial water and density of samples. Each plot in Figure 12 is calculated from the examined lignite particles from the different grades of samples investigated. The dry bulk densities of Turow lignite are in the range of 400 kg· m^{-3} and 1300 kg· m^{-3}. This corresponds to the WP_{ini} of 25% and 60%. The results of tests were found in the widespread range. This indicates that the divergent physical properties of Turow lignite, which strongly influence the drying behavior. The widely divergent dry bulk density of the Turow lignite is related to the inhomogeneous seam structure due to the sedimentary contamination of inorganic matters resulting in local high ash concentrations.

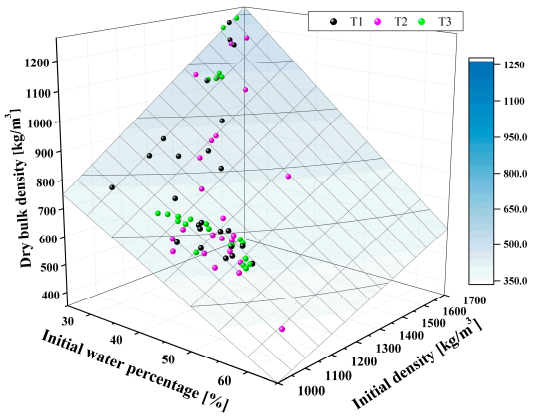

Figure 12. Correlation of WP_{ini} and initial density of samples to the measured dry bulk densities.

Figure 13 shows the correlation of the drying rate at the CDRP and WP_{ini} of the examined samples. The drying rate was also predicted with the given density of the dry matter in the lignite, using Equation (3). Plots on Figure 13 is the drying rate obtained from the drying test of 10 mm samples dried in 170 °C. The lowest drying rate is obtained with the sample that contains lowest *WP* and the highest density. This may be attributed to the higher composition of the ash in the sample. As a matter

of the fact, the drying rate of highly contaminated T1 sample can be found in this profile. A higher density of dry matter, together with the decrease of WP_{ini}, lowers the drying rate at the CDRP. With the consideration that has been shown in Table 2 and the deliberation from Figure 12, high concentration of ash may be the most influential factor deciding the tendency of lowered drying rate. In this lignite sample, the loam and quartz sands sedimentations or inorganic matters originated in the detirius coal structure seems to be the cause.

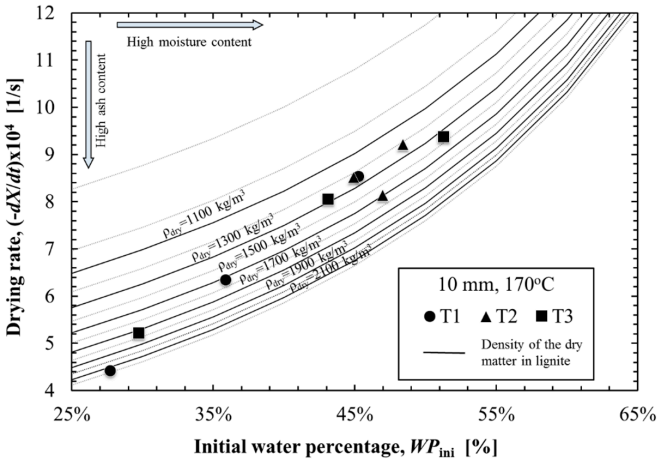

Figure 13. The influence of the WP_{ini} and lignite density (of dry matter) for the initial drying rate at the CDRP.

4.3. Evaluation of Initial and Residual Moisture Contents and Drying Time

Figure 14 shows the correlation between the initial water and the density of raw sample before drying for T1, T2 and T3 samples. Histogram chart of WP_{ini} was presented together with the correlation for each sample. The WP_{ini} spreads very widely for whole range in the figure (from 25% to 55%) and this can be seen in all the presented samples T1, T2 and T3. Samples T1 and T3 are essentially from the same seam, so they have similarity with moisture among the group of relatively large amount of initial water (37.5%–51.5%) and of lower density of raw material (1.14–1.30 g· cm^{-3}). Trend in Sample T3 distinguishes this group more clearly. The trend in Sample T1 is on the other hand rather blur and difficult to distinguish. It may be connected with the implication of contamination in the sample. Sample T3 also implies the footwall of the Seam I, this group may be seen in the other one of Figure 14c (plots gathering with small amount of WP_{ini} and high density tested samples).

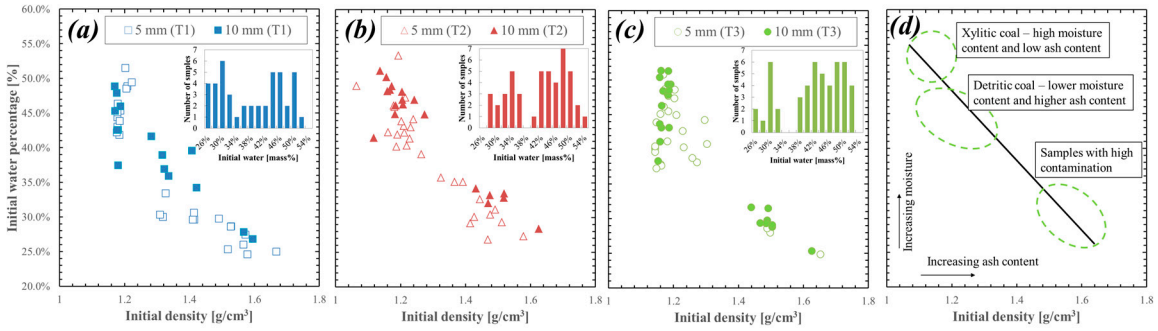

Figure 14. Correlation between the WP_{ini} (mass%) and the density of samples at the initial state for Samples: (**a**) T1; (**b**) T2; (**c**) T3; and (**d**) correlation between ash and moisture content.

Generally, Seam I of the Turoszow deposit is uniform, highly carbonized layer of the detritic coal with thin loam insertions in the footwall part. The depth is very divergent following the morphology

of the bottom layer of rocks and intensive tectonics. The thickness is in the range from 0 m at the edges to 35 m in the central part of south region; average thickness is 15 m. Between Seams I and II, loams, sands and gravels are located. Seam II, on the other hand, has the largest distribution and greatest thickness. The lignite is mostly detritic coal with thin inserts of xylitic coal; in footwall part many loam insertions and sedimentations can be found. Depth is less varied. Thickness is up to 42 m in the central part of the southern region and getting smaller toward the edges of the basin. The average thickness is 20 m [21]. This explains the correlation observed in Figure 12 for the variety of WP_{ini} and compositions expressed by the wide range of density. Sample T1, as footwall of Seam I, has many particles with high density (high ash contamination) and low moisture content. Sample T3 (Seam I) has mostly detritic lignite and several contaminated particles from footwall, but other lithotype are also observed. Seam II (Sample T2) has very diversified structure and all of the types of lignite can be observed.

Figure 15 shows the summary of the measurements: Initial and residual *WP* (WP_{ini} and WP_{res}) and drying time of 10 mm lignite particle along the tested temperature at 110, 130, 150 and 170 °C for Samples T1, T2 and T3. Individual tests were characterized by the widespread WP_{ini}, but the averaged one is more uniform among the tested samples (39%, 41% and 41% for Samples T1, T2 and T3). The averaged drying time is also similar to each other, so that their trend is exponential with the change in the tested temperature. However, their individual characteristics spread on the broad ranges. Quantification and precise evaluation must be carefully carried out for each lithotype texture of lignite. This is especially important for lignite deposit with diversified seam structure, as can be observed in the Turoszow deposit.

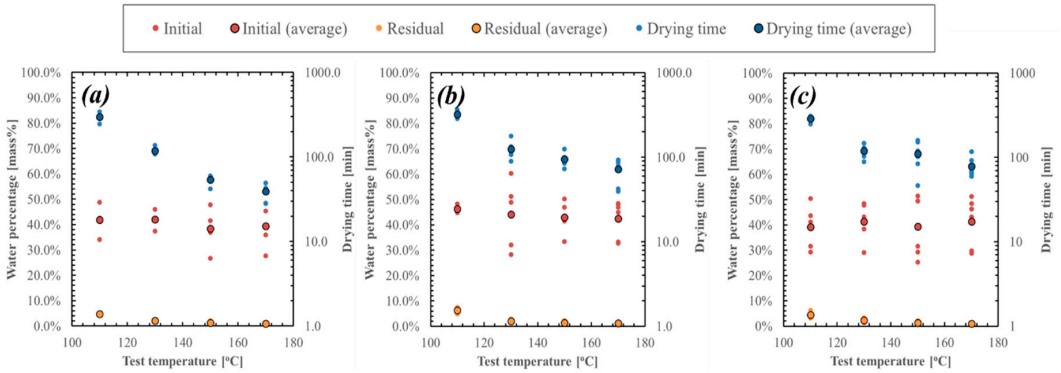

Figure 15. Initial and residual *WP*s and drying time for 10 mm particle made of Samples: (**a**) T1; (**b**) T2; and (**c**) T3.

4.4. Evaluation of the Residual Moisture Content

The residual moisture content is defined by the equilibrium moisture content curve (isobar sorption relationship) of a product in a drying medium. This is one of the important parameters describing drying process necessary for the analysis, modeling and optimization of drying system. As the WP_{ini} varies among various types of lignite, the residual moisture content observed in various drying condition is also different depending on the structure of lignite and steam temperature. As lignite from different sampling points, such as Samples T1, T2 and T3, exhibits analogical properties (Figure 14) in the terms of distribution of initial moisture content and density, it was analyzed together and the probability density of the WP_{ini} among all measured samples was checked. The observed distribution plotted in Figure 16a can be described as combination of two normal distributions, with the cross section point at WP_{ini} equals to 36%. They are identified as relatively high moisture content lignite samples (WP_{ini} higher than 36%) and lignite samples with a high ash contamination (WP_{ini} lower than 36%) (Figure 14). The residual moisture content was analyzed separately for those two groups: high ash-contaminated and relatively high moisture content lignite samples. Lignite from both groups exhibits different sorption isobars as presented in Figure 16b. The clear difference between the residual moisture content for detritic and xylitic coals pointed in Figure 14 was not observed.

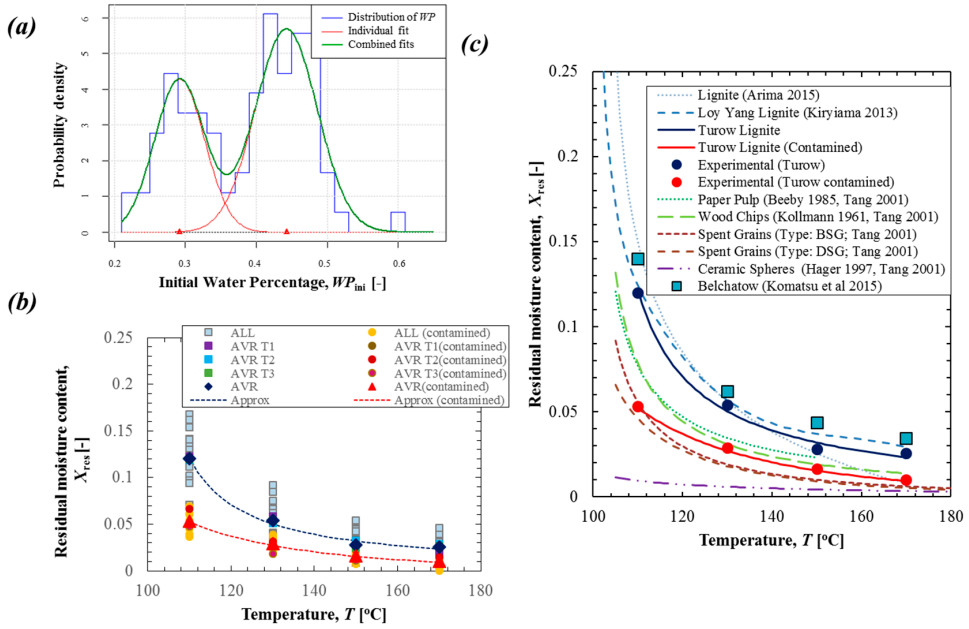

Figure 16. (**a**) Probability density of the distribution of the WP_{ini} of Turow lignite samples; (**b**) residual moisture content in Turow lignite; and (**c**) comparison of residual moisture content in various materials based on data from the literatures [9,16,18,27–30].

The experimental deliberation on equilibrium moisture content in various materials were presented by Tang and Cenkowski [27]. It was suggested that description of the temperature dependence of the equilibrium moisture content X_{res} can be approximated by the following class of functions:

$$X_{res} = k \times e^{n(T-100)^m} \quad (5)$$

where parameters k, n and m are estimated on the basis of experimental investigation. Tang and Cenkowski [27] compared the experimentally obtained equation for equilibrium moisture content of brewers' spent grains with the equations for different materials derived from various experimental results [27]. They stated that Equation (5) cannot be applied for describing the equilibrium moisture content of brown coal, as lignite has the enhanced moisture absorption capacity below 140 °C [27]. However, in this paper, it is postulated that this type of equation describes well the observed experimental results in the steam temperature above 110 °C. Due to the moisture absorption capacity, the sorption isobar in the temperature below 110 °C has to be defined by the additional dependence as it was presented in the works of Kiriyama *et al.* [16] and Arima *et al.* [9].

The final empirical formulation estimated in this study has the following form for the lignite from the Turow deposit:

$$X_{res} = 44.79 \times e^{-4.41(T-100)^{0.127}}, \text{ for } T \geqslant 110 \quad (6)$$

and in the case of the lignite from the Turow deposit with a high ash contamination:

$$X_{res} = 0.085 \times e^{-0.081(T-100)^{0.778}}, \text{ for } T \geqslant 110 \quad (7)$$

The comparison of the experimental results and the approximation by Equations (6) and (7) is presented in Figure 16b. It is visible that the residual moisture of the highly contaminated lignite (with WP_{ini} below 36%) is around twice smaller than the low ash-contaminated lignite in all conditions and it exhibits slower increase with the decrease of steam temperature.

Another formulation to describe the equilibrium moisture content in lignite is the one proposed by Kiryiama *et al.* [16], who investigated Australian Loy Yang lignite in which the WP_{ini} was 62%:

$$\begin{array}{l} X_{res} = -7.43 \times 10^{-7} \times T^3 + 3.49 \times 10^{-4} \times T^2 - 5.50 \times 10^{-2} \times T + 2.93, \text{ for } T > 110 \\ X_{res} = \frac{0.706}{T-98.6} + 6.23 \times 10^{-3}, \text{ for } 100 \leqslant T \leqslant 110 \end{array} \quad (8)$$

and by Arima *et al.* [9], who investigated brown coals with WP_{ini} in the range of 61.3%–62.8%:

$$\begin{array}{l} X_{res} = \frac{1}{100}\left(\left(\frac{3.34\times10^7}{T-103}\right)^{\frac{1}{4.33}} - 19.9\right), \text{ for } T \geqslant 104 \\ X_{res} = 0.35 - (T - 104) \times \frac{125}{400}, \text{ for } T < 104 \end{array} \quad (9)$$

Figure 16c presents the comparison of the experimental results and approximation delivered in this study with the equilibrium moisture content of lignite proposed by the studies of Kiryiama *et al.* [16] and Arima *et al.* [9]. The empirical equation proposed by this study is superior to the other experimental correlation presented in [9,16,17] in the temperature range above 110 °C and it includes and addresses the phenomenon observed in the case of lignite with high ash contamination.

Figure 16c compares additionally the equilibrium moisture content derived by Tang and Cenkowski [27] for various materials on the basis of experimental research on ceramic spheres [28], spent grains [27], wood chips [29], and paper pulp [30]. It is noticeable that the sorption isobars of lignite are higher than for other materials, except the results for the ash-contaminated Turow lignite. The lowest equilibrium moisture content is exhibited in the case of ceramic spheres. It is correlated with non-capillary porous structure of this material. This consideration may be applied to the contaminated Turow lignite and also decrease the X_{res}, where the high ash content decreases the sorption abilities. The other group of Turow lignite, which was distinguished by threshold WP_{ini} over 36%, lies on the broad range of WP_{ini} from 36% to 60%. The type of lithotype may differ this parameter and accordingly the residual moisture content. However, it is difficult clarify the correlation between lignite lithotype and their WP_{ini} due to the specific physical property of this lignite. Values of the residual moisture content are divergent among the sample tested at a single condition. It is noteworthy to mention that that the averaged residual moisture content of Turow lignite is very similar to that of Loy Yang lignite, which has around 62% of WP_{ini}. Moreover, The Belchatow lignite, which was excavated from Central Poland and has about 50% WP_{ini}, indicated a similar value. The residual moisture content of the types of lignite resulted from the lithotypes may be influenced by structure of lignite. Particularly, porosity of sample and pore size and its distribution can be concerned, which determine the surface area of the lignite. This must be further studied since the drying process involves the destruction of pores in dewatering as the shrinkage of the samples was observed. These factors can decide the total moisture content and as a result the drying rate.

5. Conclusions

The present experimental investigation focuses on detailed descriptions of drying kinetics of lignite from the Turow lignite mine in Poland. Lignite particles of 5 mm and 10 mm in diameter were used for drying test in superheated steam in the temperature range of 110 °C–170 °C in atmospheric conditions. Observations include correlated changes in moisture content, drying rate, temperature profiles and appearance on the surface of the sample. In the literature, the descriptions of superheated steam drying process can be found. However, they focus on single grade of lignite excavated from one certain seam of a mine. The present study pointed out the necessity of the investigations on the drying kinetics found on the sample taken from the seam with divergent lithotype textures. The basic correlations among lithotypes of detric, xylitic, xylo-detritic, detro-xylitc and highly contaminated coal with the drying kinetic were presented. The general dependencies of drying time, drying rate, temperature gradient, cracking and shrinkage behavior and differences between samples of chosen lithotype textures were discussed. However, the quantitative classification has to be developed and the method of averaging the drying parameters for seam consistent of various lithotype textures has to be proposed.

The attempts to derive the formulas considering the influence of lignite properties for the drying rate in the CDRP and the residual moisture have been attempted. Thermodynamic quantification of the drying rate at the CDRP was successfully carried out. Although the total drying time strongly depends on the tested sample: its WP_{ini} and physical properties, which were divergent due to the lithotype texture extracted from the Turow mine. As it was presented, the residual moisture also depends on the physical properties of the tested lignite; the most influential factor considered in the present paper was the level of ash contamination. The empirical formula was proposed to evaluate the residual moisture content in terms of the dependence on the superheated steam temperature.

In the presented research, significant differences in the drying behavior, drying rate and drying time for lignite originated from one geographical location and different geological origins were observed. The further quantification and precise evaluation must be carried out for each lithotype texture of lignite in order to enable the design of superheated steam drying system. This is especially important for lignite deposit with diversified seam structures, as can be observed in the Turoszow deposit.

Acknowledgments: The present study was financially support by the Japan Coal Energy Center (JCOAL) and by the Polish National Centre for Research and Development (NCBR Project: I_POL-JAP,SSD-4-LRC).

Author Contributions: Shozo Kaneko and Janusz S. Szmyd conceived and designed the research, Anna Sciazko, Yosuke Komatsu, Marcin Zakrzewski and Taro Akiyama performed the experiments, Anna Sciazko and Yosuke Komatsu analyzed the data, Yosuke Komatsu wrote the paper, Akira Hashimoto consulted the technical issues in the experimentation, Akira Hashimoto, Shozo Kaneko, Naoki Shikazono, and Yoshinori Kobayashi consulted the content.

Conflicts of Interest: The authors declare no conflicts of interest.

Abbreviations

CDRP	Constant drying rate period
DDRP	Decreasing drying rate period
JIS	Japanese Industrial Standards
LLS-2	The second group of Lusatian lignite seam
LRC	Low-rank coal
SSFBD	Superheated steam fluidized bed drying (dryer)
ŚLS-3	The third group of Ścinawa lignite seam

References

1. Kozłowski, Z. Present situation and prospects for lignite in the Polish power-generation industry. *Appl. Energy* **2003**, *74*, 323–329. [CrossRef]
2. Allardice, D.J. The Water in Brown Coal. In *The Science of Victorian Brown Coal: Structure, Properties and Consequence for Utilization*; Durie, R.A., Ed.; Butterworth-Heinemann Ltd.: Oxford, UK, 1993; pp. 103–150.
3. Fushimi, C.; Kansha, Y.; Aziz, M.; Mochidzuki, K.; Kaneko, S.; Tsutsumi, A.; Matsumoto, K.; Yokohama, K.; Kosaka, K.; Kawamoto, N.; *et al.* Novel drying process based on self-heat recuperation technology. *Dry Technol.* **2010**, *29*, 105–110. [CrossRef]
4. Osman, H.; Jangam, S.V.; Lease, J.D.; Mujumdar, A.S. Drying of low-rank coal (LRC)—A review of recent patents and innovations. *Dry Technol.* **2011**, *29*, 1763–1783. [CrossRef]
5. Li, J.; Liang, Q.-C.; Bennamoun, L. Superheated steam drying: Design aspects, energetic performances, and mathematical modeling. *Renew. Sustain. Energy Rev.* **2016**, *60*, 1562–1583. [CrossRef]
6. Hamawand, I.; Yusaf, T.; Bennett, J. Study and modelling drying of banana slices under superheated steam. *Asia Pac. J. Chem. Eng.* **2014**, *9*, 591–603. [CrossRef]
7. Hamawand, I.; Pereira, W.; Eberhard, F.; Antille, D.L. Issues related to waste sewage sludge drying under superheated steam. *Polish J. Chem. Technol.* **2015**, *17*, 5–14. [CrossRef]
8. Liu, Y.; Kansha, Y.; Ishizuka, M.; Fu, Q.; Tsutsumi, A. Experimental and simulation investigations on self-heat recuperative fluidized bed dryer for biomass drying with superheated steam. *Fuel Process. Technol.* **2015**, *136*, 79–86. [CrossRef]

9. Arima, K.; Tsuchiyama, Y.; Suzuki, T.; Sawatsubashi, T.; Kakigami, H.; Kinoshita, M.; Ishii, H. Drying characteristics of wet brown coal particles in a steam fluidized bed. *Kagaku Kogaku Ronbunshu* **2015**, *41*, 100–106. (In Japanese) [CrossRef]
10. Law, C.L.; Mujumdar, A.S. Fludized Bed Dryer. In *Handbook of Industrial Drying*; Mujumdar, A.S., Ed.; CRC Press: Boca Raton, FL, USA, 2006; pp. 174–201.
11. Jangam, S.V.; Karthikeyan, M.; Mujumdar, A.S. A Critical Assessment of industrial coal drying technologies: Role of energy, emissions, risk and sustainability. *Dry Technol.* **2011**, *29*, 395–407. [CrossRef]
12. Bongers, G.D.; Jackson, W.R.; Woskoboenko, F. Pressurised steam drying of Australian low-rank coals: Part 1. Equilibrium moisture contents. *Fuel Process. Technol.* **1998**, *57*, 41–54. [CrossRef]
13. Bongers, G.D.; Jackson, W.R.; Woskoboenko, F. Pressurised steam drying of Australian low-rank coals: Part 2. Shrinkage and physical properties of steam dried coals, preparation of dried coals with very high porosity. *Fuel Process. Technol.* **2000**, *64*, 13–23. [CrossRef]
14. Looi, A.Y.; Golonka, K.; Rhodes, M. Drying kinetics of single porous particles in superheated steam under pressure. *Chem. Eng. J.* **2002**, *87*, 329–338. [CrossRef]
15. Shi, Y.C.; Li, J.; Li, X.Y.; Wu, J.; Wu, M.G.; Li, S.; Wang, H.Y.; Zhao, G.J.; Yin, F.J. Experimental study on super—Heated steam drying of lignite. *Adv. Mater. Res.* **2011**, *347*, 3077–3082. [CrossRef]
16. Kiriyama, T.; Sasaki, H.; Hashimoto, A.; Kaneko, S.; Maeda, M. Experimental observations and numerical modeling of a single coarse lignite particle dried in superheated steam. *Mater. Trans.* **2013**, *54*, 1725–1734. [CrossRef]
17. Kiriyama, T.; Sasaki, H.; Hashimoto, A.; Kaneko, S.; Maeda, M. Size dependence of the drying characteristics of single lignite particles in superheated steam. *Metall. Mater. Trans. E* **2014**, *1*, 349–363. [CrossRef]
18. Komatsu, Y.; Sciazko, A.; Zakrzewski, M.; Kimijima, S.; Hashimoto, A.; Kaneko, S.; Szmyd, J.S. An experimental investigation on the drying kinetics of a single coarse particle of Belchatow lignite in an atmospheric superheated steam condition. *Fuel Process. Technol.* **2015**, *131*, 356–369. [CrossRef]
19. Pikon, J.; Mujumdar, A.S. Drying of Coal. In *Handbook of Industrial Drying*; Mujumdar, A.S., Ed.; CRC Press: Boca Raton, FL, USA, 2006; pp. 993–1018.
20. PGE. Turow Lignite Mine. Available online: http://www.kwbturow.pgegiek.pl/ (accessed on 20 January 2015).
21. Widera, M. Changes of the lignite seam architecture—A case study from Polish lignite deposits. *Int. J. Coal Geol.* **2013**, *114*, 60–73. [CrossRef]
22. Wagner, M. *Brunatny Węgiel Bitumiczny ze Złóż Turów i Bełchatów w Świetle Badań Petrograficzno—Chemicznych i Sedymentologicznych*; Wydawnictwo Centrum Podstawowych Problemów Gospodarki Surowcami Mineralnymi i Energią PAN: Kraków, Poland, 1996. (In Polish)
23. Widera, M. Macroscopic lithotype characterisation of the 1st Middle-Polish (1st Lusatian) Lignite Seam in the Miocene of central Poland. *Geologos* **2012**, *18*, 1–11. [CrossRef]
24. Kopp, O.C.; Harris, L.A. Initial volatilization temperatures and average volatilization rates of coal—Their relationship to coal rank and other characteristics. *Int. J. Coal Geol.* **1984**, *3*, 333–348. [CrossRef]
25. Umar, D.F.; Usui, H.; Daulay, B. Effects of processing temperature of hot water drying on the properties and combustion characteristics of an Indonesian low rank coal. *Coal Prep.* **2005**, *25*, 313–322. [CrossRef]
26. Ticleanu, N.; Scradeanu, D.; Popa, M.; Milutinovici, S.; Popa, R.; Preda, I.; Ticleanu, M.; Savu, C.; Diaconita, D.; Barus, T.; *et al.* The relation between the lithotypes of Pliocenne coals from Oltenia and thier main quality characteristics. *Bull. Czech Geol. Surv.* **1999**, *74*, 169–174.
27. Tang, Z.; Cenkowski, S. Equilibrium moisture content of spent grains in supherheated steam under atmospheric pressure. *Trans. ASAE* **2001**, *44*, 1261–1264. [CrossRef]
28. Hager, J.; Hermansson, M.; Wimmerstedt, R. Modelling steam drying of a single porous ceramic sphere: Experiments and simulations. *Chem. Eng. Sci.* **1997**, *52*, 1253–1264. [CrossRef]
29. Kollmann, F.F.P. High temperature drying: Research, application and experience in Germany. *For. Prod. J.* **1961**, *11*, 508–515.
30. Beeby, C.; Potter, O.E. Steam Drying. In *Drying '85*; Springer: Berlin/Heidelberg, Germany, 1985; pp. 41–58.